Performance of Turbofan Engine Nacelle Design for Boeing 777X Using Computational Fluid Dynamics Analysis

Nova Zena Vania*and Andrew Ragai Henry Rigit
Department of Mechanical and Manufacturing Engineering, Universiti Malaysia Sarawak, Jalan Datuk Mohammad Musa, 94300 Kota Samarahan, Sarawak, Malaysia

Abstract

The efficient design of turbofan engine nacelles is critical for enhancing aircraft performance and supporting sustainable aviation goals. This study investigates the aerodynamic and thermal performance of various nacelle configurations for the Boeing 777X GE9x engine, focusing on innovative cooling strategies and drag reduction. Using Computational Fluid Dynamics simulations, nacelle shapes of varying lengths (10 m and 5.5 m), including long and short nacelles with and without chevrons, as well as an optimized ultra-short nacelle, were analyzed under cruise conditions. Models were developed using MATLAB and SolidWorks, and simulations were performed in ANSYS Fluent. Results indicate that the long nacelle with chevrons provided the best overall thermal and aerodynamic performance among the conventional designs, reducing drag and block fuel consumption by 10.13%. However, the optimized ultra-short nacelle, developed using a hybrid NSGA-Non Dominated Sorting Genetic Algorithm II and *fmincon- Find Minimum of Constrained optimization approach using MATLAB, achieved a significantly lower drag coefficient and reduced block fuel consumption by 80.13%. These findings demonstrate the potential of advanced nacelle designs to improve heat dissipation, reduce aerodynamic drag, and lower emissions, aligning with stringent EASA standards and contributing to sustainable aviation advancements.*

Keywords: *Engine Nacelle Design, Boeing 777X, Nacelle Shape, Computational Fluid Dynamics (CFD), Chevron, Optimization.*

1. Introduction

The aviation industry continues to push the boundaries of performance, safety, and environmental responsibility. Among the critical components contributing to these objectives is the engine nacelle, a streamlined structure that houses the engine while enhancing the aerodynamic characteristics of the aircraft. Beyond its protective function, the nacelle plays a key role in reducing aerodynamic drag, mitigating noise, and shielding the engine from environmental hazards such as debris, lightning, and foreign object ingestion. In modern high-bypass turbofan engines, such as those powering the Boeing 777X, thermal management has become a significant design challenge. These engines generate considerable heat, which, if not adequately managed, can adversely affect engine performance, increase specific fuel consumption (SFC), and raise greenhouse gas emissions. According to Nikolaidis et al. [1], a 1% pressure loss in the bypass duct may lead to a 2% increase in fuel usage, highlighting the sensitivity of engine efficiency to nacelle design and airflow characteristics. Climate change introduces additional complexity, including increased occurrences of

* Corresponding author.
E-mail address: novazena.53.nzv@gmail.com

Manuscript History:
Received 25 September, 2025, Revised 15 October, 2025, Accepted 17 October, 2025, Published 31 October, 2025

https://doi.org/10.33736/jaspe.10944.2025

e-ISSN: 2289-7771

clear-air turbulence (CAT) due to warmer temperatures and weakened jet streams. CAT poses a growing operational risk by increasing unplanned fuel consumption, emissions, and potential flight delays [2-3].

These environmental pressures demand nacelle designs that are not only aerodynamically optimized but also capable of effective thermal regulation under varying atmospheric conditions. This study proposes a novel nacelle design aimed at improving cooling performance and aerodynamic efficiency for high-bypass turbofan engines. The research focuses on the GE9x engine used in the Boeing 777X and employs Computational Fluid Dynamics (CFD) simulations to evaluate the thermal and aerodynamic impacts of changes in nacelle shape and length. By improving heat dissipation characteristics, the proposed design seeks to reduce fuel consumption and emissions, contributing to more sustainable and efficient aircraft operations. The scope of the research is limited to the geometric design aspects of the nacelle, excluding material properties. The findings aim to contribute to the broader field of sustainable aerospace design by providing insights into nacelle geometry optimization for next-generation aircraft engines.

2. Modelling approach and boundary condition

This study employs quantitative and simulation methods to optimize nacelle designs for the Boeing 777X by varying shape and length to minimize engine temperature, fuel consumption, and emissions. Design and analysis were conducted using MATLAB, Autodesk SolidWorks 2024, and ANSYS Fluent, accessed via UNIMAS student licenses. Modeling and simulations were performed on a workstation with an Intel i7-9750H CPU, NVIDIA GTX GPU, 16 GB RAM, running Windows 11.

MATLAB was used to generate trailing edge profiles based on Class Shape Transformation (CST). These profiles were refined in SolidWorks, and aerodynamic performance was analyzed using CFD simulations in ANSYS Fluent. Optimized nacelle designs from CFD results were further processed in MATLAB using NSGA-II and fmincon algorithms for multi-objective optimization. Design parameters and engine specifications were adopted from the literature review, adhering to EASA standards (CS-E800, CS-25.1091, CS-25.1191), focusing on aerodynamic drag and pressure recovery. This methodology enables the identification of the most efficient nacelle configuration for the Boeing 777X.

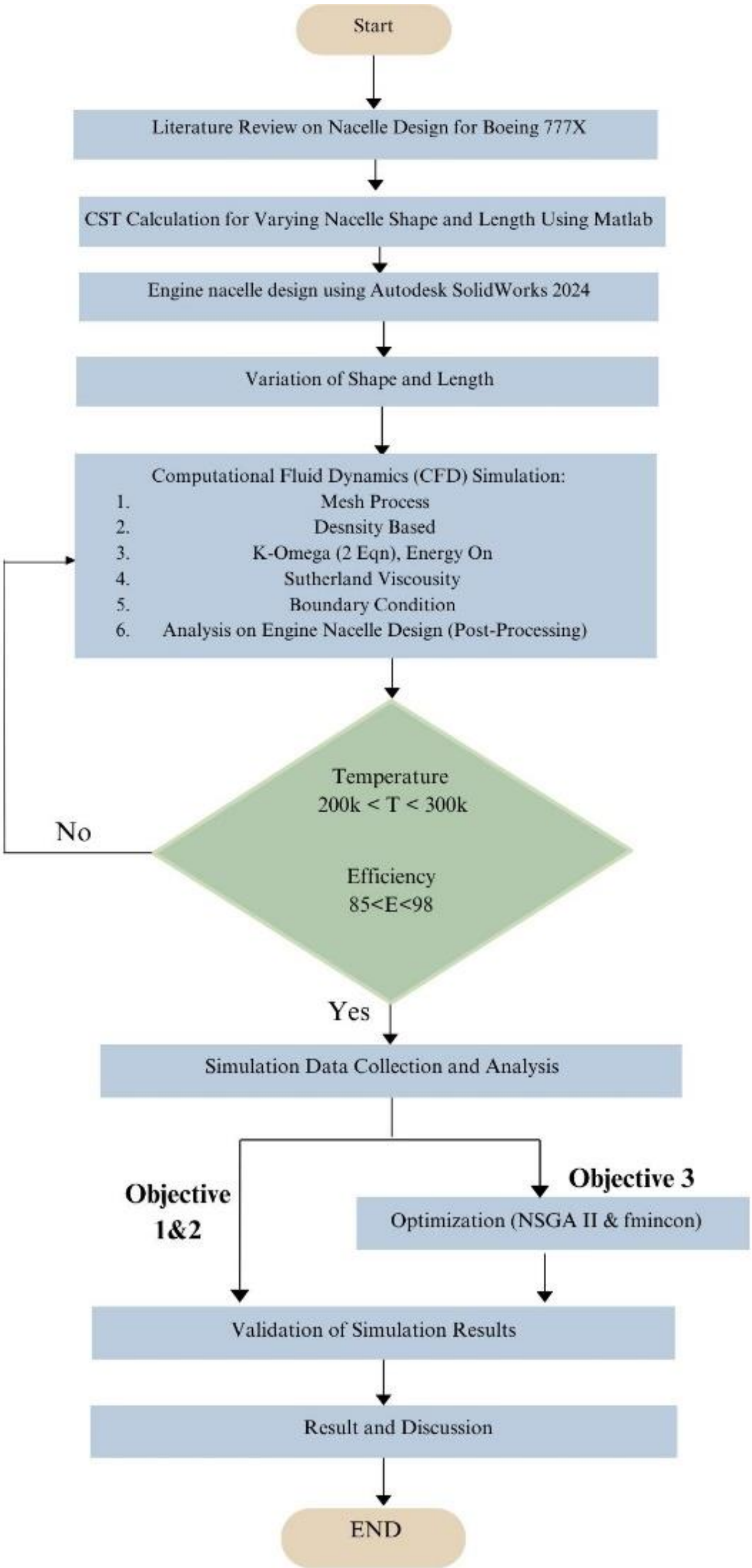

Figure 1. Flow chart of the research methodology

2.1. Procedure for nacelle shape formulation and computational simulation

The nacelle designs will be created in Autodesk SolidWorks. However, before being imported into Autodesk SolidWorks, the trailing edge is produced by using MATLAB.

2.1.1. Design procedure

The nacelle geometry was generated using the Class Shape Transformation (CST) method, which has been widely applied for aerodynamic shape parameterization due to its flexibility and simplicity in defining complex geometries. The base shape function B(ψ) is expressed as:

$$B(\psi) = l_{nac} + \psi(r_{te} - r_{hi}) \tag{1}$$

Where $\psi = \frac{x}{l_{nac}}$ represents the nondimensional coordinate along the nacelle length, a denotes the leading edge, and b denotes the trailing edge position, both in meters. The class function defines the overall geometric behavior of the nacelle profile.

$$C(\psi) = \psi^{a}(1-\psi)^{b} \tag{2}$$

The final shape function $S(\psi)$ is expressed as a Bernstein Polynomial Expansion:

$$S(\psi) = \sum_{i=0}^{n} bc_i \, \psi^{i}(1-\psi)^{n-1}. A_i \tag{3}$$

Where n is the degree of the polynomial and A_i represents the coefficient that defines the contribution of each term to the overall shape. The complete surface is represented by the combination of all functions as:

$$y(x) = B(\psi) + C(\psi) + S(\psi) \tag{4}$$

The mass-slow capture ratio (MFCR) is subsequently determined using the relationship:

$$MFCR = \frac{A_c}{A_f} \tag{5}$$

(Equations 1-5 adapted from Kulfan, 2007)

After completing the nacelle design, an EASA number is chosen to adjust the nacelle based on the qualifications and standards to make sure the design meets airworthiness requirements [13].

Table 1. Design parameter of engine nacelle [12]

Parameter	Values	Description
r_{hi}	1.3194 m	Highlight radius
r_{te}	1.20197 m	Trailing edgement
l_{nac}	10 m | 5.5 m	Nacelle length
r_{if}	0.12526 m	Initial forebody radius
β	11°	Boat tail angle
d_i	2.423 m	Inlet diameter
d_m	2.85 m	Maximum diameter
d_e	2.40394 m	Exit diameter

Based on the class shape transformation (CST), the shape of the trailing edge of the nacelle design is formed for both shapes using Matlab, as shown in Figure 2.

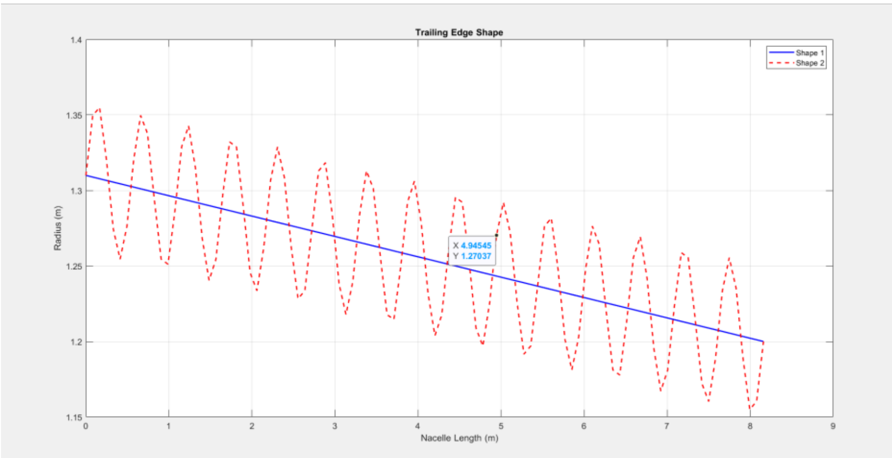

Figure 2. Trailing edge shape from MATLAB

The trailing edge retrieved from MATLAB is used as the guideline to generate the full shape of the nacelle. This form of the nacelle will be imported into Autodesk SolidWorks to refine the shape using the revolved Boss/Base command. There are two types of nacelles, with lengths of 10 m and 5.5 m, and with/out chevron nacelle as shown in Figure 3.

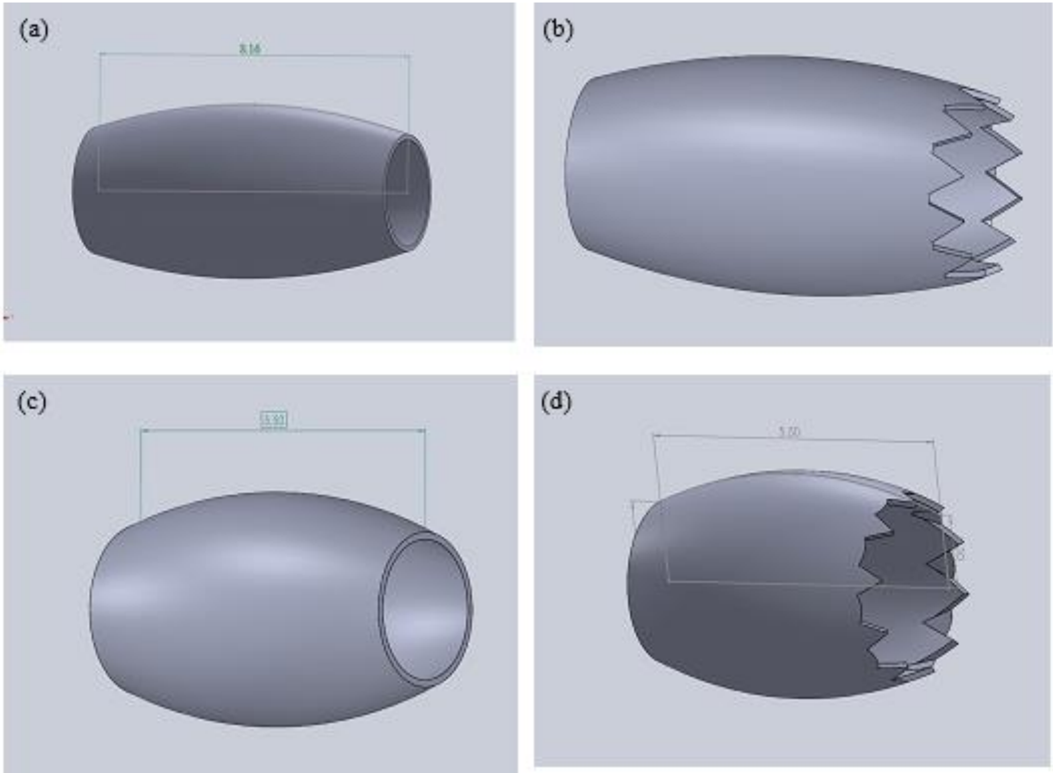

Figure 3. Non-axisymmetric engine nacelle a) Chevron long nacelle with chevron, b) Long shape without chevron, c) Short nacelle without, d) Short nacelle with chevron

Each nacelle configuration is situated within a cubic computational domain, as shown in Figure 4, which is to establish the external flow boundaries and maintain consistent aerodynamic conditions during the numerical simulation. The nacelle domain is cuboid in form. The dimensions of the computational domain are determined based on the nacelle geometry, with values of 10 m in length, 15 m in width, and 10 m in height. These dimensions are selected to ensure that the flow around the nacelle is able to fully develop and that the influence of the domain boundaries on the aerodynamic results is minimized. This approach follows common CFD practices for external aerodynamic simulations.

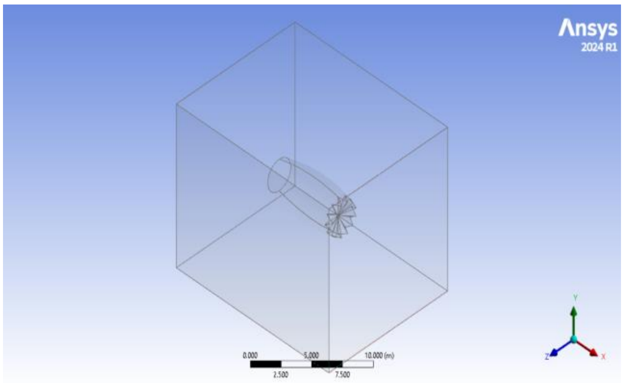

Figure 4. Fluid domain for engine nacelle designs

2.1.2. Simulation procedure

After the model stage is completed, the next step is the simulation of the model by using Ansys Fluent. In this case, the objective of the simulation is to analyze aerodynamic drag, heat dissipation, and engine efficiency. The nacelle design models are drawn to scale based on measurements provided by researchers to enhance accuracy and precision. However, due to limited access to the original data, the author estimates some values for simulation. The simulation is assumed to be in steady-state flow. The simulation process comprises three phases: pre-processing, numerical solution, and post-processing. The flow of simulation of the nacelle design is shown in Figure 5.

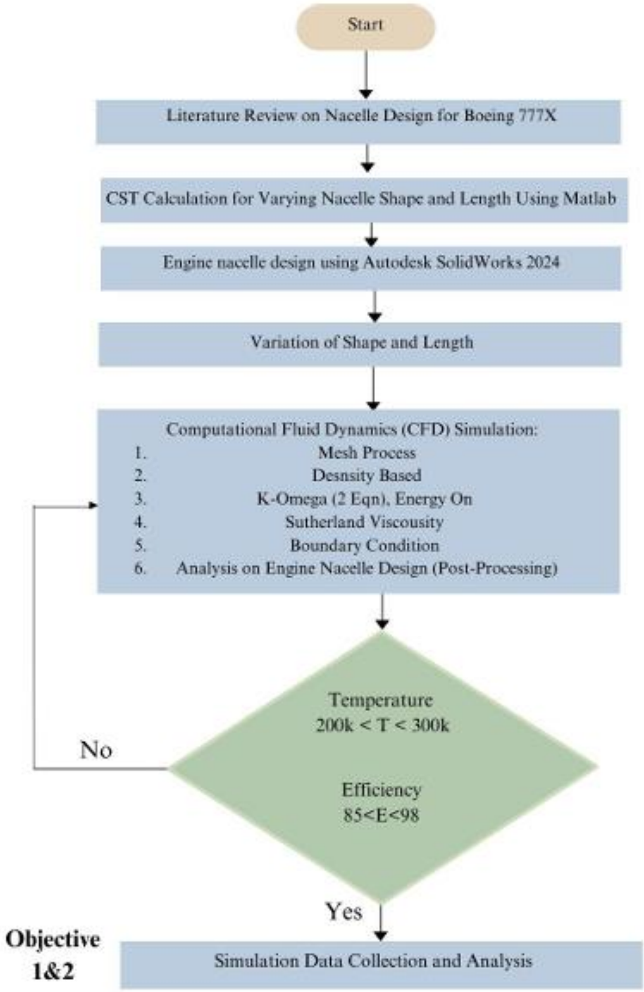

Figure 5. Flowchart for nacelle design simulation

2.1.2.1. Meshing configuration and settings

The meshing configuration for all turbofan engine nacelle models was maintained uniformly to ensure consistency and comparability of the simulation results. This subsection outlines the specific meshing parameter applied during the preprocessing stage of the nacelle design analysis. As summarized in Table 2, the mesh was generated using an element size of 66a mm with high smoothing, employing a skewness-based quality metric and advancing front meshing method. The detailed mesh distribution and topology for the turbofan engine nacelle are illustrated in Figure 6.

Table 2. Meshing settings for all engines' nacelle models

Element Order	**Adjustment**
Element Size	664 mm
Smoothing	High
Mesh Metric	Skewness
Triangle Surface Mesher	Advancing Front

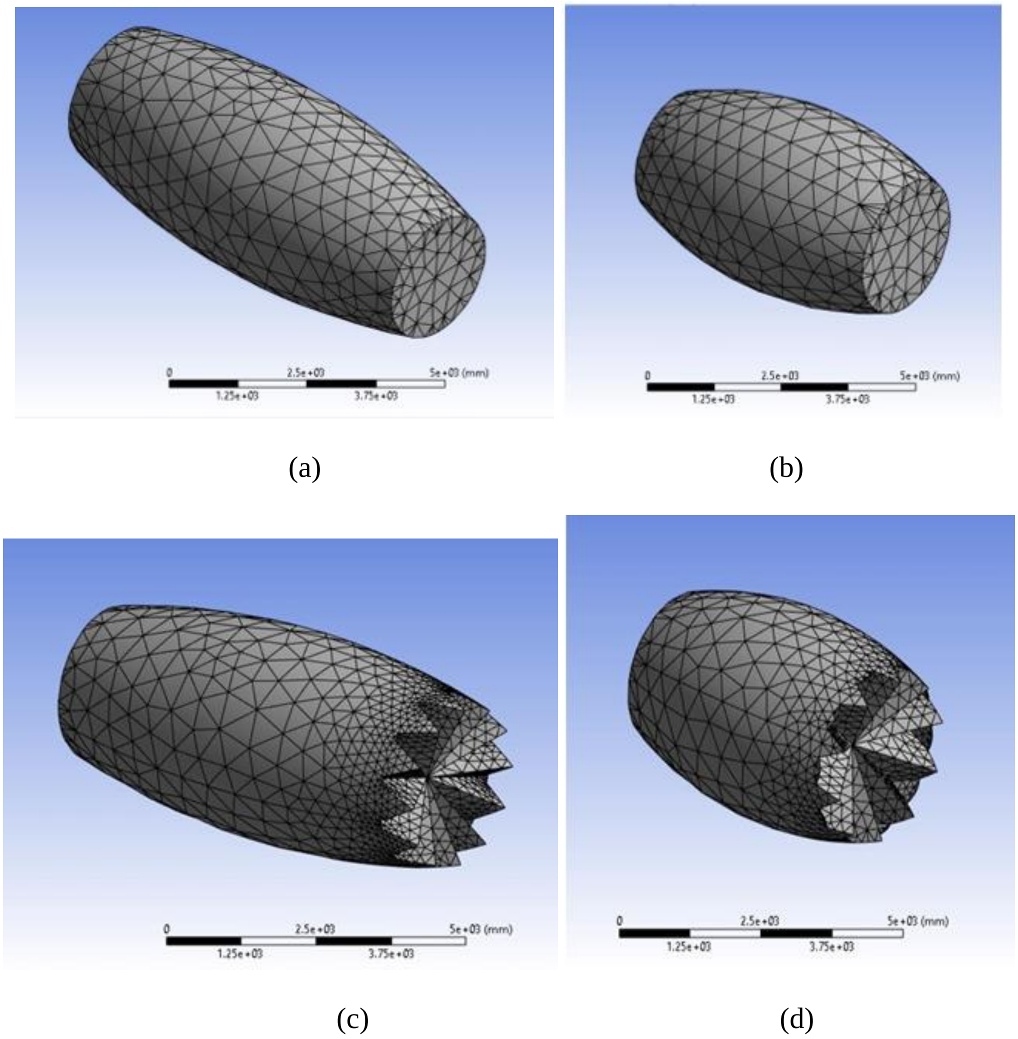

Figure 6. Meshing of each shape of nacelle: (a) Long nacelle without chevron, (b) short nacelle without chevron, (c) Long nacelle with chevron, (d) Short nacelle with chevron

2.1.2.2. Boundary conditions and parameters used in ANSYS Fluent

Boundary conditions in ANSYS Fluent consist of various types, such as inlet and outlet flow boundaries, wall boundaries, velocity inlet boundaries, pressure inlet boundaries, and others. The parameter used during the simulation is shown in Table 3.

Table 3. Parameters for CFD solver in ANSYS Fluent [6]

Solver	Type: Density-based Velocity formulation : Absolute Time : Steady
Model	Energy : On Viscous : SST k-omega (2 eqn)
Fluid Materials	Air Density : Ideal-gas Viscosity : Sutherland
Boundary Conditions	**For temperature and pressure** Inlet : Pressure Inlet Gauge Total Pressure : 25000 Pa, 40000 Pa Supersonic/Initial Gauge Pressure : 94500 Thermal : 973.15K, 288.15 Wall : Stationary wall, No Slip Outlet : Pressure outlet Gauge pressure outlet : 15000 Pa, 34300 Pa **For drag coefficient** Inlet : Velocity-Inlet Velocity Magnitude : 250.81 m/s Supersonic/Initial Gauge Pressure : 94500 Pa Thermal 973.15 K Outlet : Pressure Outlet Gauge pressure outlet : 15000 Pa
Reference Value	Compute from : Inlet Velocity : 250.81 m/s
Solution Methods	Formulation : Implicit Flux type : Roe-FDS Gradient : Least squares cell-based Flow : Second Order Upwind Turbulent Kinetic Energy : Second Order upwind Specific Dissipation Rate : Second Order Upwind
Solution Initialization	Standard Initialization Compute from : inlet Reference frame : relative to cell zone
Run Calculation	Number of Iterations : 1000 Reporting Interval : 1 Profile Update Interval : 1

After completing the simulations, the aerodynamic drag of the nacelle is obtained, which allows the determination of engine efficiency. The thrust generated by the engine is identified. The fuel efficiency due to each nacelle can be determined using this formula:

$$D = \frac{1}{2}\rho V^2 S C_d \tag{6}$$

Where
$\rho = Density\ of\ the\ air\ (kg/m^2$
$V = Velocity\ (\frac{m}{s})$
$S = Wing\ Area\ (427.35\ m^2)$
$C_d = Drag\ Coefficient$

Once the nacelle drag is calculated, the fuel flow can be determined using:

$$\text{Fuel Flow} = (D)(TSFC) \tag{7}$$

Where D is drag and TSFC is thrust specific fuel consumption

After calculating the required fuel flow, the block fuel can be determined using the equation:

$$\text{Block Fuel} = (\text{Fuel Flow})(\text{Time}) \tag{8}$$

$$\text{Time} = \frac{3000}{488} = 6.15\ hours\ \text{(time to fly 3000 nmi)}$$

Finally, engine efficiency can be evaluated using the appropriate efficiency formula:

$$\text{Percent Change} = \left(\frac{Block\ Fuel - Baseline\ Block\ Fuel}{Baseline\ Block\ Fuel}\right) \times 100\% \tag{9}$$

After obtaining the percentage changes or engine efficiency, the result is compared with other researchers' results, which are from NASA data [13].

2.2. Procedure for simulation and optimization of ultra-short nacelle design

To achieve an optimized ultra-short nacelle configuration, a series of procedures was conducted, many of which mirrored those applied in Objectives 1 and 2, as illustrated in Figure 5. The initial nacelle geometry was generated following the methodology established in the previous objectives. Equations 1 to 5 were employed to construct the trailing edge profile, which was subsequently refined using SolidWorks for enhanced geometric accuracy. However, the shape of optimized ultra-short nacelle design is a bit different due to the combination and modification of the short nacelle and modified chevron, as shown in Figure 7. The computational simulation was carried out under the same conditions and input parameters as in Objectives 1 and 2, as shown in Table 2. The simulation process for the optimized ultra-short nacelle is summarized in the flowchart shown in Figure 8. Fuel efficiency was calculated based on equations 6 through 9.

In order to do optimization, a hybrid approach was implemented, which is combination of NSGA-II for multi-objective optimization with fmincon for constrained nonlinear optimization. It is used to identify the optimal nacelle design configuration. The expected outcomes of the optimization include minimized drag coefficient, optimized temperature distribution, improved fuel efficiency, and an aerodynamically efficient trailing edge shape.

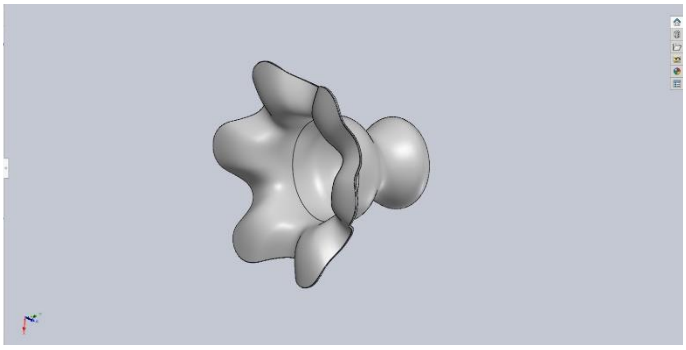

Figure 7. Model for Optimized Ultra-short Nacelle Design

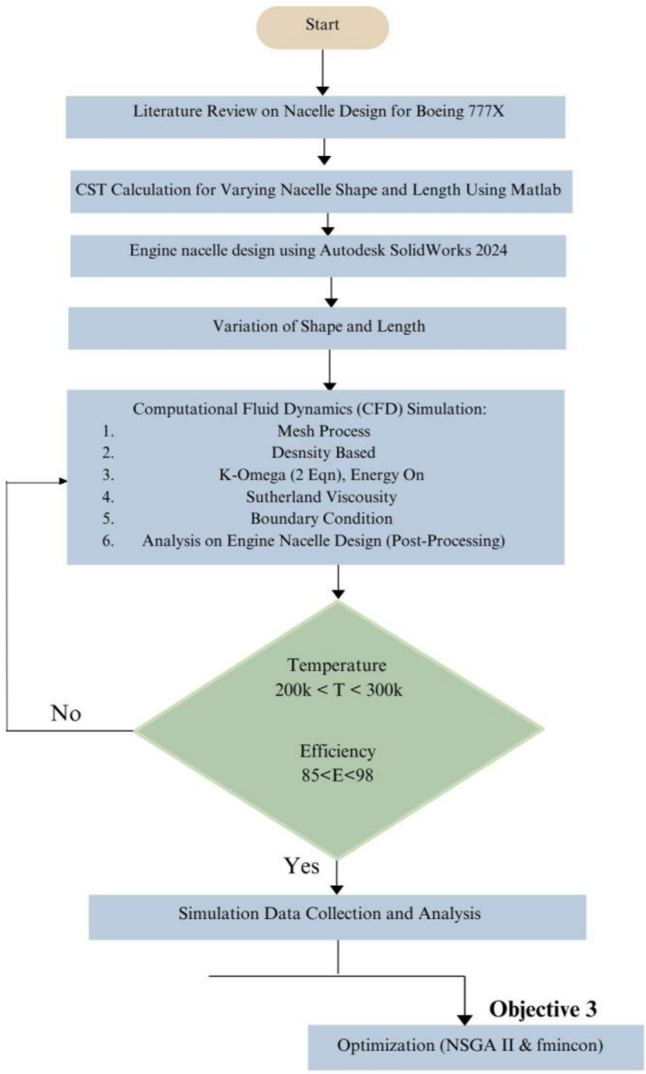

Figure 8. Flow Simulation of optimized ultra-short nacelles design

3. Results and discussion

This section presents the results obtained from the computational fluid dynamics (CFD) simulations performed to analyze the aerodynamic performance of different nacelle configurations for the Boeing 777X. The primary objective of the test was to evaluate how nacelle length and the presence of chevrons affect the pressure distribution, drag coefficient, and overall aerodynamic efficiency of the engine nacelle. The simulation was conducted at a velocity of 250.81 m/s, an altitude of 11 278 meters, and an angle of attack of 0º, representing the cruise condition of a Boeing 777X**.**

3.1 Temperature results of four nacelles

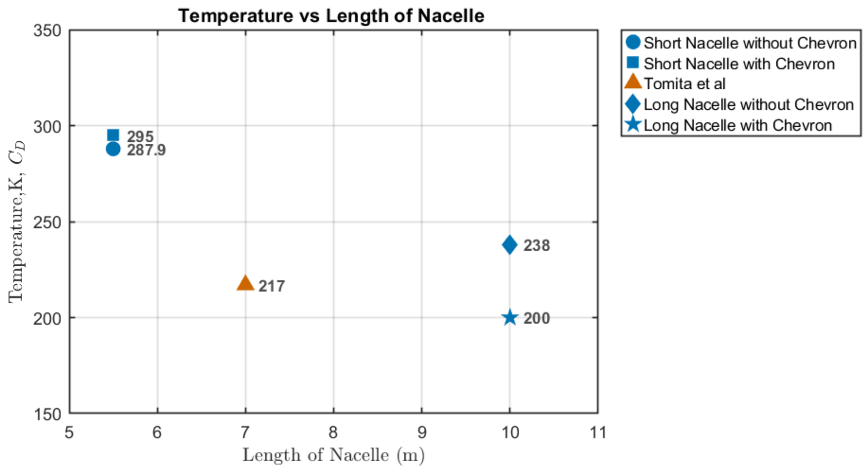

Figure 9. Comparison of the temperature obtained for each nacelle shape from the current simulation with other researchers

The results highlight the critical influence of nacelle geometry on thermal behavior under cruise conditions as shown in Figure 10. Tomita et al [8] reported a 217 K temperature for a 7 m nacelle, serving as a benchmark. In contrast, the short nacelle without chevrons (5.5 m) reaches 287.9 K (circle marker), significantly higher due to limited duct length, which restricts flow deceleration and thermal dissipation. The addition of chevrons to this short nacelle further increases the temperature to 295 K (rectangle marker), indicating that chevron-induced turbulence and vortex mixing, while beneficial for noise reduction and flow control [4], [5] can generate localized heating when insufficient downstream length is available for dissipation. The long nacelle without chevrons (10 m) registers a reduced temperature of 238 K (diamond marker), slightly above Freede's case, due to enhanced flow diffusion and passive cooling over the extended duct. Notably, the long nacelle with chevrons achieves the lowest observed temperature of 200 K (pentagon marker), demonstrating that chevrons significantly improve thermal performance when coupled with a sufficiently long nacelle. This configuration allows turbulent mixing to occur within the duct length, promoting uniform flow and more effective heat dispersion, aligning with findings in [6] and [7].

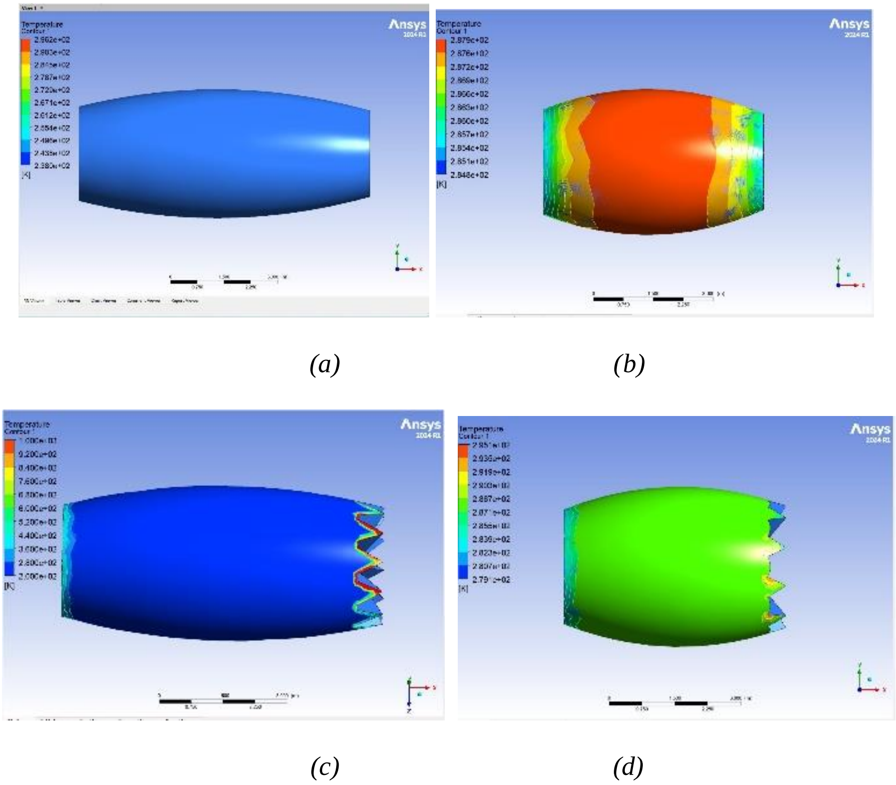

Figure 10. Comparison of the temperature of turbofan engine nacelle designs: a) Long shape without chevron, b) Short nacelle without chevron, c) Long nacelle with chevron, d) Short nacelle with chevron

3.2. Pressure results of four nacelles

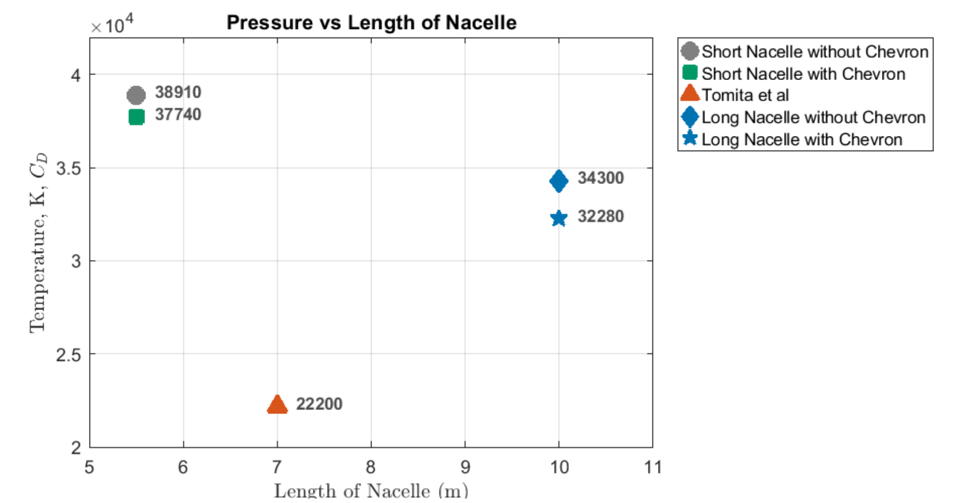

Figure 11. Comparison of the pressure obtained for each nacelle shape between the current simulation and published data

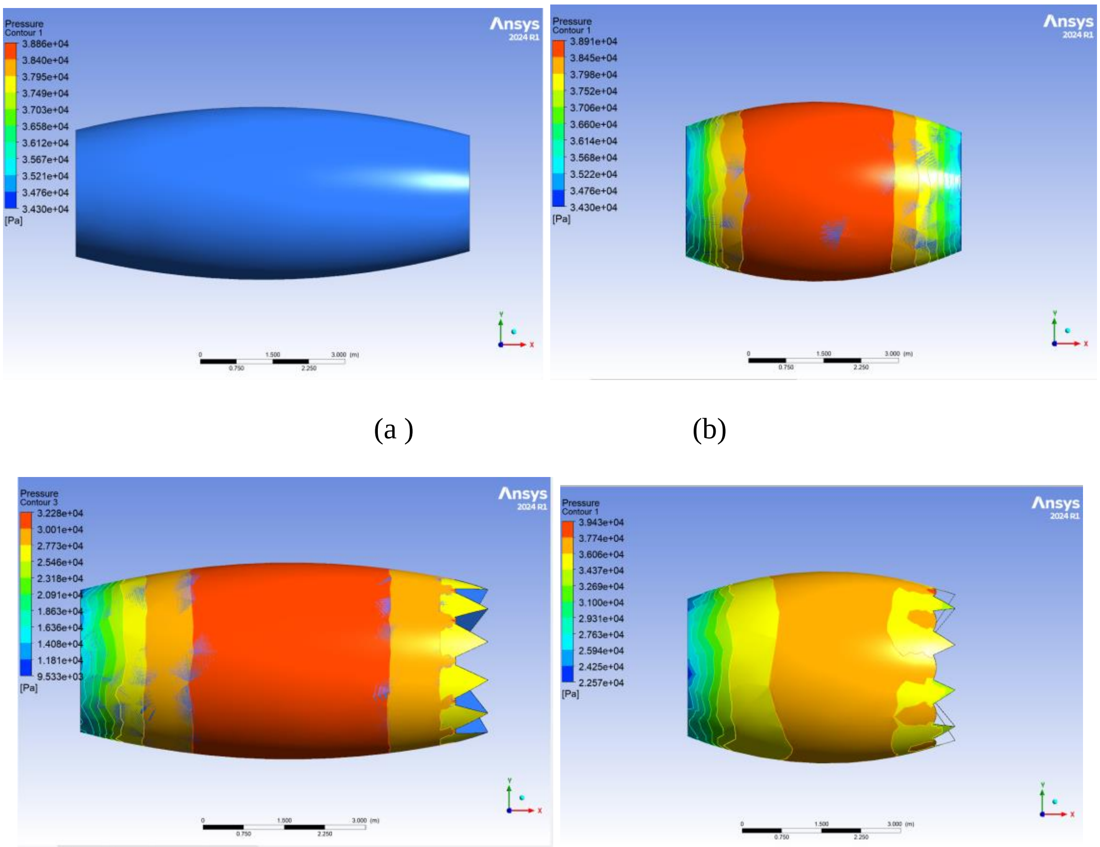

(a)　　(b)

(c)　　(d)

Figure 12. Comparison of the pressure of turbofan engine nacelle designs: a) long shape without chevron, b) short nacelle without chevron, c) long nacelle with chevron, d) short nacelle with chevron

Figure 11 compares the simulated pressure distributions of various nacelle configurations with those reported in previous studies. The results emphasize the significant impact of nacelle length and geometry, particularly the presence of chevrons on static pressure behavior along the nacelle surface.

In general, longer nacelles result in lower overall pressure due to smoother flow deceleration and enhanced pressure recovery. The configuration by Tomita *et al.* [8], indicated by a triangular marker, reported the lowest pressure at 22,200 Pa, reflecting highly efficient flow management. In contrast, the short nacelle without chevrons (circular marker) exhibited the highest pressure at 38,910 Pa due to abrupt boundary layer deceleration and limited surface area for pressure diffusion.

The introduction of chevrons, designed to improve shear-layer mixing and mitigate flow separation, demonstrated measurable benefits. The short nacelle with chevron (rectangular marker) showed a reduced pressure of 37,740 Pa, while the long nacelle with chevron recorded the lowest pressure among the current designs at 32,280 Pa, as shown in Figure 12. This reduction is attributed to the chevrons generating streamwise vortices that enhance ambient air entrainment and reduce wake pressure, consistent with findings by Bridges and Envia [9] and Tam and Parrish [10].

Although all tested configurations showed higher pressures than those of Tomita et al.[8] reference, the long nacelle with chevrons proved to be the most aerodynamically effective among the present designs. This highlights the synergistic benefit of combining extended nacelle length with chevron-induced vortex structures to enhance pressure recovery and overall flow control.

3.3. Drag coefficient results of four nacelles

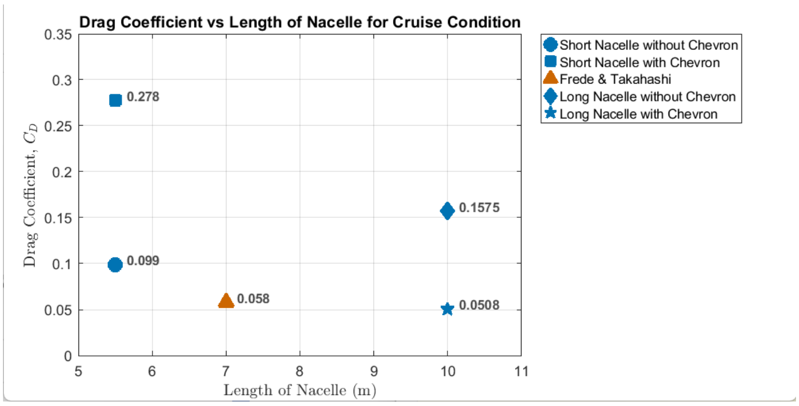

Figure 13. Comparison of the drag coefficient obtained for each nacelle shape from the current simulation with other researchers

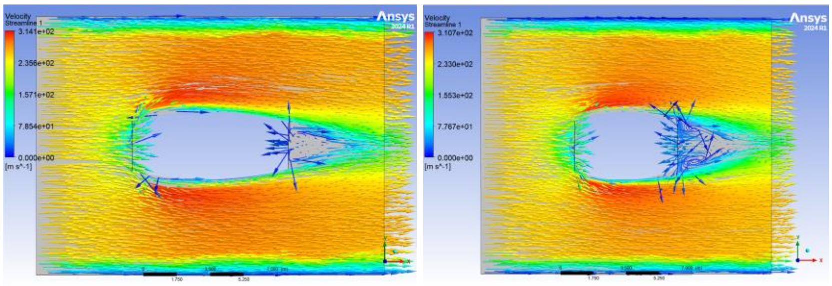

(a) *(b)*

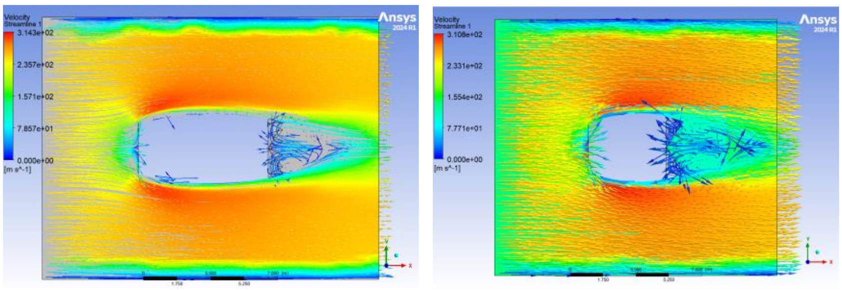

(c) *(d)*

Figure 14. Comparison of the airflow of turbofan engine nacelle designs: a) long shape without chevron, b) short nacelle without chevron, c) long nacelle with chevron, d) short nacelle with chevron

Figure 14 presents a comparative analysis of the drag coefficients obtained from the current Computational Fluid Dynamics (CFD) simulations against the experimental findings of Frede and Takashi[15] under cruise conditions. The configuration studied by Frede and Takashi[15], denoted by a triangle marker in Figure 13, recorded a drag coefficient (C_d) of 0.058. In contrast, the short nacelle without chevrons yielded a higher drag coefficient of 0.099 (circular marker), while the short nacelle with chevrons produced the highest drag coefficient among all tested configurations at 0.278.

The observed differences in drag performance are largely attributed to variations in nacelle length and the presence of chevron structures. Specifically, the long nacelle without chevrons achieved a drag coefficient of 0.1575 (parallelogram marker), suggesting improved flow development over the shorter designs, but still exhibiting considerable wake formation.

In contrast, the long nacelle with chevrons achieved the lowest drag coefficient of 0.0508 (pentagon marker), slightly outperforming the Frede and Takashi [15] configuration. This enhanced aerodynamic behavior is primarily due to the synergistic effects of extended nacelle length and chevron-induced flow control. The chevrons, which are serrated structures at the trailing edge, generate streamwise vortices that enhance shear layer mixing and reduce turbulence intensity at the nozzle exit [9-10]. These controlled vortices help delay boundary layer separation, suppress recirculating flow regions, and reduce adverse pressure gradients. As a result, the wake is more organized and narrow, leading to a significant reduction in pressure (form) drag.

Moreover, chevrons contribute to improved flow symmetry and velocity reattachment at the nacelle aft-body, promoting smoother flow detachment and improved pressure recovery. The long nacelle provides sufficient surface length for gradual velocity development and supports laminar-to-turbulent transition without premature separation. When combined, the extended nacelle geometry and chevron features yield a stable, high-momentum wake with reduced turbulence and lower drag as schematically illustrated in Figure 3.5 and validated by the minimum drag coefficient observed in this study.

3.4. Fuel efficiency results for four nacelles

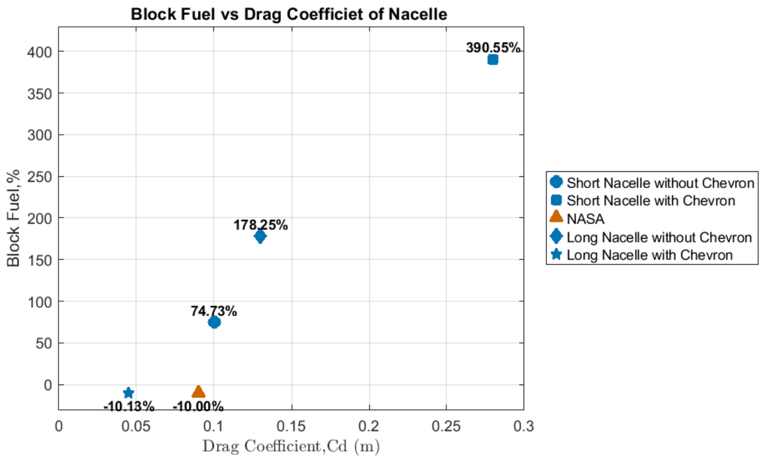

Figure 15. Comparison of block fuel obtained for each nacelle shape from the current simulation with other researchers

Figure 15 shows the correlation between drag coefficient and block fuel consumption for different nacelle configurations. The long nacelle with chevrons achieved the best performance, reducing fuel usage by 10.13%, slightly outperforming NASA's UEET reference configuration at –10.00% [11]. This improvement is attributed to the chevron's ability to enhance jet mixing, reduce shear-layer separation, and improve pressure recovery, leading to lower aerodynamic drag [9], [10].

In contrast, the short nacelle with chevrons showed the highest fuel consumption (+390.55%), followed by the long nacelle without chevrons (+178.25%) and the short nacelle without chevrons (+74.73%). These results emphasize that nacelle length alone does not ensure fuel efficiency; effective flow control features like chevrons are essential.

The performance aligns with NASA's UEET findings, which highlighted the benefits of optimized BPR, advanced shaping, and nacelle integration [11]. The chevron-enhanced long nacelle replicates these aerodynamic principles, achieving superior fuel efficiency through reduced drag and improved flow control.

3.5. Optimized ultra-short nacelle

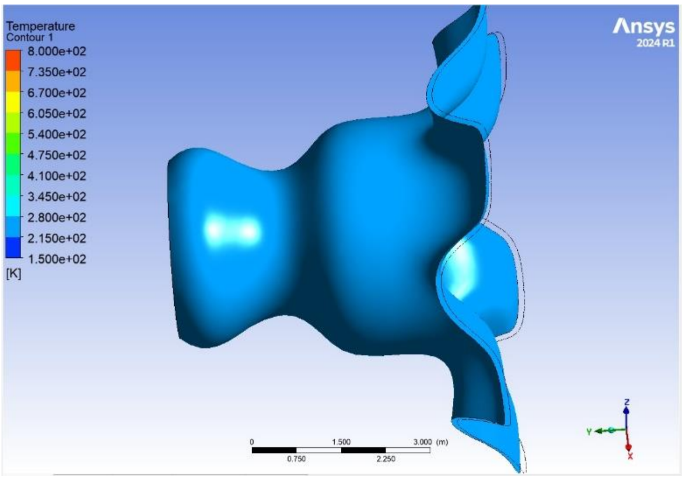

Figure 16. Temperature distribution for ultra-short nacelle

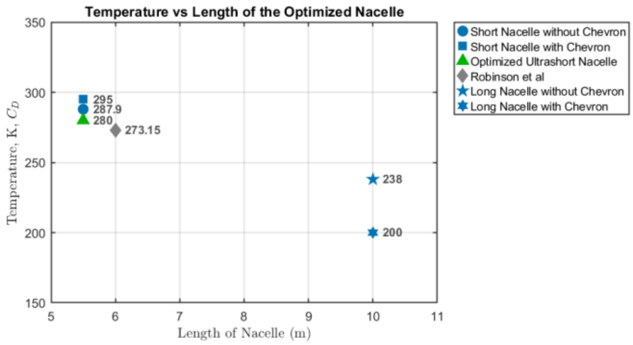

Figure 17. Comparison of the temperature obtained for the ultra-short nacelle from the current simulation with Robinson et al

Figure 17 shows that the optimized ultrashort nacelle exhibits a higher surface temperature (280 K) than the configuration by Robinson et al. (273.15 K), due to its compact geometry, which may induce flow separation and reduce cooling efficiency. As noted by Tejero et al. [6], non-monotonic curvature, particularly near the afterbody and trailing edge, can lead to localized heat accumulation. A key factor in thermal performance is the chevron geometry at the trailing edge. The broader chevron on the optimized nacelle enhances core-bypass mixing, promoting early thermal dissipation and reducing downstream eddies [22]. This results in a lower temperature than short nacelles without chevrons (295 K) and with chevrons (287.9 K). While long nacelles show the lowest temperatures (238 K and 200 K) due to extended flow development, the ultrashort nacelle's chevron compensates by improving thermal mixing, consistent with findings by Bridges and Brown [4] on vortex breakdown and thermal spreading.

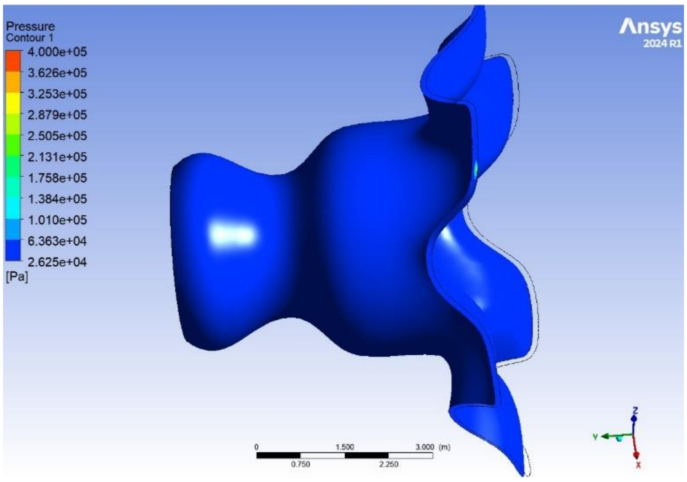

Figure 18. Pressure distribution for ultra-short nacelle

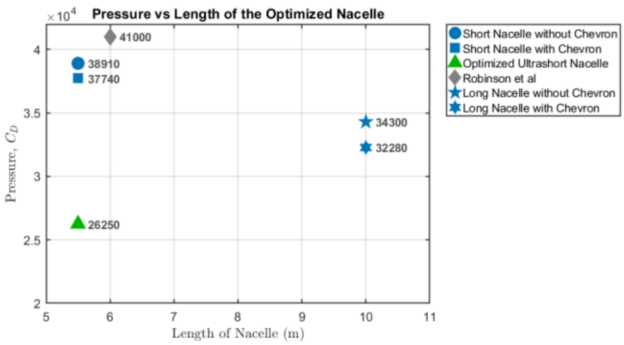

Figure 19. Comparison of pressure obtained for ultra-short nacelle from current simulation with Robinson et al

Figure 18 shows the pressure distribution on the optimized ultra-short nacelle, where the dark blue contour indicates a uniform low pressure of 26,250 Pa near the trailing edge, attributed to the broader chevron geometry. This design enhances jet and ambient air mixing, reducing turbulence and vortex formation as noted by Bridges and Brown [4]. A pressure rise at the midsection results from sharp curvature, causing a recirculation zone that increases local static pressure and lowers aerodynamic efficiency. Elevated pressure near the trailing edge stems from turbulent wake interactions and vortex shedding, which the chevron helps mitigate through smoother mixing.

Figure 19 compares nacelle pressures, showing that the optimized ultra-short nacelle achieves the lowest pressure (26,250 Pa) versus Robinson et al.'s 41,000 Pa and other designs. The chevron's vortex disruption and enhanced mixing reduce drag and improve aerodynamic performance.

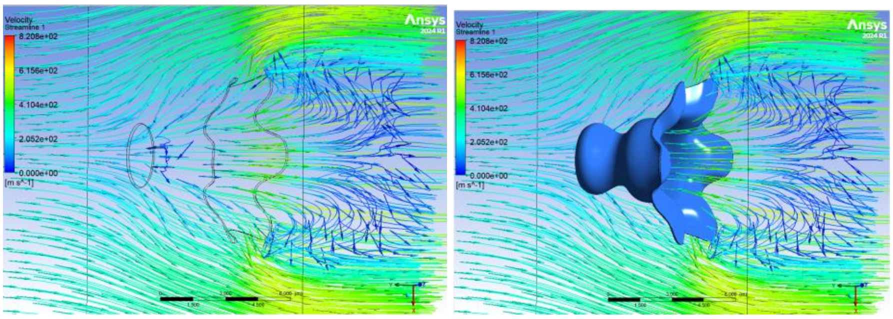

(a) (b)

Figure 20. Drag coefficient result for optimized ultra-short nacelle a) Airflow of ultra-short nacelle, b) Airflow exit from ultra-short nacelle

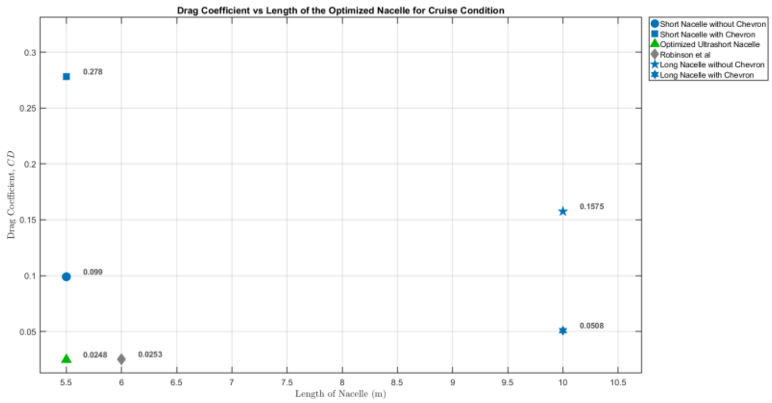

Figure 21. Comparison of Drag Coefficient for Cruise Condition: Ultra-Short Nacelle (Current Simulation vs. Robinson et al.)

Figure 20 shows the airflow distribution around the ultra-short nacelle, highlighting smooth flow attachment and minimal separation at the inlet and trailing edges, which reduces drag. With a length-to-diameter ratio of 0.35, this nacelle is more compact than traditional designs, reducing wetted area and drag CD=0.0248C_D = 0.0248CD=0.0248, compliant with EASA standards [12], [13]. The trailing edge features chevrons that smooth curvature transitions, minimizing flow separation and boundary layer distortion [6].

At the inlet, flow recirculation and vortices arise due to sharp curvature, causing adverse pressure gradients and boundary layer separation, as seen in Figure 21. Conversely, the trailing edge shows outward flow, indicating effective wake management and pressure recovery. The use of Class Shape Transformation (CST) enables precise curvature control, maintaining flow attachment and reducing vortex formation [14, 5].

Figure 21 compares drag coefficients under cruise conditions, with the optimized ultra-short nacelle achieving CD=0.0248, CD = 0.0248, CD=0.0248, outperforming Robinson et al.'s CD=0.0253, CD = 0.0253, CD=0.0253 [6]. The broader trailing edge with chevrons stabilizes the wake, lowers base drag, and supports thermal exhaust integration without compromising aerodynamics [14, 6]. These results confirm that geometric optimization, especially at the trailing edge, significantly improves aerodynamic efficiency [6].

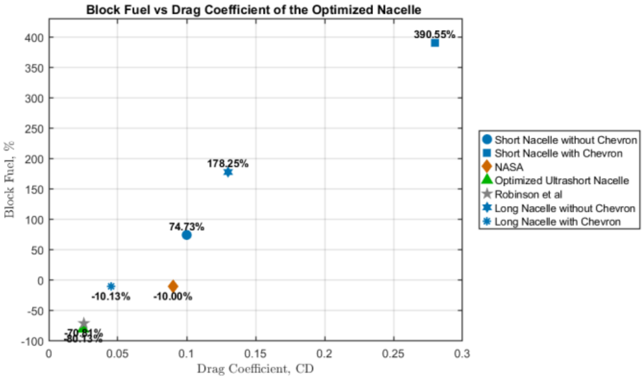

Figure 22. Comparison of block fuel obtained for each nacelle shape from optimized ultra-short nacelle with other researchers

The optimized ultra-short nacelle achieves a significant block fuel reduction of 80.13%, outperforming Robinson et al.'s configuration at 78.81% and far exceeding NASA's 10.00% reduction. This improvement reflects superior aerodynamic efficiency achieved by minimizing drag (CD=0.024, 8CD = 0.0248CD=0.0248) and optimizing the nacelle's length-to-diameter ratio (L/D) and fan pressure ratio (FPR), as well as integration with the airframe.

The NASA study highlights reducing wave and profile drag by refining L/D to prevent shock formation. The optimized nacelle's shorter length and expanded trailing-edge chevrons promote even airflow distribution, reducing drag and enhancing fuel economy in compliance with EASA standards. In contrast, configurations such as Short Nacelle with Chevron (+390.55%) and Long Nacelle without Chevron (+178.25%) show large increases in block fuel consumption due to aerodynamic inefficiencies and higher wetted areas.

4.0 Conclusion

The study explored the aerodynamic and thermal performance of various nacelle configurations for the Boeing 777X under cruise conditions that focus on four key designs, such as long and short nacelles, with and without chevrons, and optimized ultra-short nacelle. The findings highlighted that nacelle shape and the presence of chevrons significantly impact temperature distribution, pressure behavior, drag coefficient, and fuel efficiency. The long nacelle with chevrons demonstrated superior aerodynamic characteristics, achieving the lowest drag coefficient (Cd = 0.0508), lowest temperature (200 K), and improved pressure recovery, resulting in a 10.13% block fuel reduction. However, due to its increased weight, material usage, and cost, this configuration may not be the most practical for all aircraft applications. In contrast, the optimized ultra-short nacelle, developed through CFD simulation and multi-objective optimization using NSGA-II and Constrained optimization, which is the fmincon algorithm, offers a more practical alternative.

Despite its compact size, it recorded a drag coefficient of 0.0248, lower than both experimental references and previous designs, while also reducing block fuel consumption by 80.13%. The broader chevron at the trailing edge played a crucial role in enhancing flow mixing, stabilizing wake regions, and mitigating thermal hotspots. One of the limitations encountered during this study is the restricted availability of accurate data for the nacelle design. The original design document that provided real dimensions and specifications was not accessible, resulting in reliance on estimated or generic data. Consequently, some calculations and simulation results may lack precision and may not fully reflect actual conditions. For future work, it is recommended to obtain access to authentic nacelle design documents from aerospace manufacturers or organizations that can provide the actual specifications. Access to real design data increases the accuracy of calculations and simulations, leading to more reliable and practical results. Additionally, integrating experimental validation methods could help overcome data limitations and improve the accuracy of the study.

Acknowledgements

The authors would like to express their sincere gratitude to the Faculty of Engineering, Universiti Malaysia Sarawak and Hornbill Skyways Sdn. Bhd. for providing the facilities, resources, and academic support for this research. Special thanks to Dr Mohamad Iskandar bin Jobli and Mr Yong Chen Yie for the assistance.

Conflict of Interest

We declare no conflicts regarding the publication of the study.

References

[1] Nikolaidis, G., Kyprianidis, A. R. & Singh, A. (2020). Impact of bypass duct pressure loss on engine performance, *Journal of Aerospace Engineering*, 34(2), 235–244.

[2] Prosser, I., Sheridan, P., & Williams, J. (2023). Trends in clear-air turbulence related to climate variability. *Atmospheric Science Letters, 24*(1), 1–9. https://doi.org/10.1029/2023GL103814

[3] Foudad, A., Khalil, A. & T. Bouziani, T. (2024).Clear-air turbulence: New patterns and implications for aviation, *Journal of Aviation and Climate Dynamics*,12(3), 87–94.

[4] Bridges, J. & Brown, C. (2004). Effect of chevron nozzles on jet noise, NASA TM-2004-213107.

[5] Cican, G., Deaconu, M., & Crunteanu, D.-E. (2021). Impact of using chevrons nozzle on the acoustics and performances of a micro turbojet engine. *Applied Sciences, 11*(11), 5158. https://doi.org/10.3390/app11115158

[6] Tejero, F., Robinson, M., MacManus, D. G., & Sheaf, C. (2019). Multi-objective optimisation of short nacelles for high bypass ratio engines. *Aerospace Science and Technology, 91*(1), 410–421. https://doi.org/10.1016/j.ast.2019.02.014

[7] General Electric, "GE9X: World's largest and most efficient jet engine," Tech. Doc., 2023.

[8] Tomita, J. T., Bringhenti, C., Pozzani, D., Barbosa, J. R., de Jesus, A. B., de Almeida, O., & Oliveira, G. L. (2005). Overview on nacelle design. *Proceedings of COBEM 2005: 18th International Congress of Mechanical Engineering*, Ouro Preto, MG, Brazil, November 6–11, 2005. ABCM. https://doi.org/10.1115/GT2006-91212

[9] Bridges, J. &Envia, E. (2006). Noise measurements of chevron nozzles on a high bypass ratio turbofan engine," *AIAA Journal*, 44(12), 2879–2888.

[10] Tam, C. K. W. & Parrish, S. A. (2008). Noise control by chevrons on jet engines, *AIAA Journal*, 46(10), 2500–2510..

[11] Daggett, D. L., Kawai, R., & Friedman, D. (2003). *Blended wing body systems studies: Boundary layer ingestion inlets with active flow control* (NASA/CR-2003-212670). National Aeronautics and Space Administration. https://ntrs.nasa.gov/archive/nasa/casi.ntrs.nasa.gov/20030067749.pdf

[12] Silva, V. T. (2020). *Aerodynamic design and experimental investigation of short nacelles for future turbofan engines* [Licentiate thesis, Chalmers University of Technology]. Department of Mechanics and Maritime Sciences, Chalmers University of Technology. https://research.chalmers.se/publication/520370

[13] EASA. (2023, January 30). *Easy Access Rules for Large Aeroplanes (CS-25) – Revision from January 2023*. https://www.easa.europa.eu/en/document-library/easy-access-rules/online-publications/easy-access-rules-large-aeroplanes-cs-25?page=40

[14] Millot, G., Scholz, O., Ouhamou, S., Becquet, M., & Magnabal, S. (2018, March). *Development of a 3D CFD aerodynamic optimization tool and application to engine air intake design.* In *Proceedings of the 53rd 3AF International Conference on Applied Aerodynamics (AERO2018)* (FP25-AERO2018). Salon de Provence, France. https://www.researchgate.net/publication/346970547

[15] Frede, K. C. & Takahashi, T. T. (2020), Computational methods for the preliminary design of engine-nacelle placement on transonic aircraft, *AIAA Scitech 2020 Forum*, Orlando, FL. doi: 10.2514/6.2020-1956.

[16] Kulfan, B. M. (2007). A universal parametric geometry representation method—'CST', *45th AIAA Aerospace Sciences Meeting and Exhibit*, Reno, NV, USA, Jan. 8–11, 2007. American Institute of Aeronautics and Astronautics. doi: 10.2514/6.2007-62

[17] Robinson, M., MacManus, D. G., Christie, R., Sheaf, C., & Grech, N. (2020). Nacelle design for ultra-high bypass ratio engines with CFD-based optimisation. *Aerospace Science and Technology*, *113*, 106191. https://doi.org/10.1016/j.ast.2020.106191